Fully integrated PCR-capillary electrophoresis microsystem for DNA analysis

Eric T. Lagally,[a] Charles A. Emrich[b] and Richard A. Mathies*[abc]

[a] UC Berkeley/UC San Francisco Joint Bioengineering Graduate Group, University of California, Berkeley, CA 94720, USA
[b] UC Berkeley Biophysics Graduate Group, University of California, Berkeley, CA 94720, USA
[c] Department of Chemistry, University of California, Berkeley, CA 94720, USA.
E-mail: rich@zinc.cchem.berkeley.edu

A fully integrated genomic analysis microsystem including microfabricated heaters, temperature sensors, and PCR chambers directly connected to capillary electrophoretic separation channels has been constructed. Valves and hydrophobic vents provide controlled and sensorless sample positioning and immobilization into 200 nL PCR chambers. The use of microfabricated heating and temperature sensing elements improves the heating and cooling rates for the PCR reaction to 20 °C s^{-1}. The amplified PCR product, labeled on-column with an intercalating fluorescent dye, is injected into the gel-filled capillary for electrophoretic analysis. Successful sex determination using a multiplex PCR reaction from human genomic DNA is demonstrated in less than 15 min. This device is an important step toward a microfabricated genomic microprocessor for use in forensics and point-of-care molecular medical diagnostics.

Introduction

Recent years have seen great progress in the development of microfabricated systems for use in chemistry and biology.[1] Specifically, integrated systems capable of combining several conventional molecular biology processes on μL–nL devices promise reduction of the time, size, and cost of performing genetic analyses. The goal of such work is to develop a completely integrated device capable of conducting an entire genetic analysis, from the introduction of raw sample to the determination of a genotype. One of the most critical steps in such a process is the specific amplification of a very small amount of initial genetic material. The most popular method for such amplification is the polymerase chain reaction (PCR).[2] The advantages of PCR include exponential amplification using only two DNA primers, a relatively simple reaction sequence of iterative cycling between three temperatures, and the high fidelity with which the DNA can be amplified. However, as conventionally practiced, PCR suffers from slow thermal transfer through macroscopic tubes and samples resulting in long assay times (2–2.5 h) and a large and costly sample volume.

By integrating PCR onto microfabricated devices we can resolve the key limitations of conventional PCR. Early microfabricated PCR reactors were developed by Northrup *et al.*,[3] and also by Wilding *et al.*,[4] but these devices were not integrated with other sample preparation or analysis steps. An integrated PCR-CE microdevice was first developed in our group, and consisted of a silicon reaction chamber attached to a glass capillary electrophoresis (CE) analysis chip.[5] This device was capable of amplifying 10 μL of sample in 15 min from a template concentration of 10^6 copies μL^{-1}. Subsequent work has been conducted in silicon,[6–8] glass,[9,10] and glass capillaries,[11,12] and included both static[6,7,9–16] and flow-through[17,18] systems as well as contact and non-contact heating.[15] Some drawbacks to these methods, however, include high template concentrations necessary in some cases,[17] inability to integrate into a fluorescence detection system,[7,17] or a relatively large

sample volume.[9,10] Subsequent work in our group has yielded a monolithic integrated PCR-CE system with valves and vents for sample positioning and immobilization, chamber volumes of 200–280 nL, and cycling times of only 10 min.[19] We have recently used this device to demonstrate successful stochastic PCR to the single-template molecule limit, the ultimate in PCR sensitivity.[20]

Despite this excellent performance, our previous devices used commercial heaters and thermocouples manually applied to the back side of the glass chip that resulted in indirect temperature sensing and limited heating and cooling rates due to impaired thermal transfer. The manual placement of the temperature components also introduced problems with reproducibility. Here, we have fabricated an integrated PCR-CE device including microfabricated heaters and resistance temperature detectors (RTDs) within the PCR chambers. These added components improve the overall thermal transfer from the heating element to the PCR chamber, increase heating and cooling rates, and increase the accuracy of the temperature measurement. Heating and cooling rates are now 20 °C s^{-1}, and 20 PCR cycles are complete in only 10 min. These heating and cooling rates are within the range 2.5–70 °C s^{-1} reported for devices in which the heating element is in contact with the PCR chamber.[3–10,13,14,16,18] Although our temperature ramp rates are slower than non-contact devices,[11,12,15] our device is the first to provide an entire integrated analysis on a chip. We illustrate the utility of this new microdevice by performing a multiplex sex determination from human genomic DNA.

Materials and methods

Device design

The mask design used for fabrication of the PCR-CE device is presented in Fig. 1. The device consists of eight parallel PCR-CE systems. Each PCR chamber is connected to a loading port

DOI: 10.1039/b109031n

through a microfluidic valve. These valves are similar to those developed by Anderson *et al.*,[21] except that our design has a much smaller dead volume of only 50 nL. Each valve consists of a main chamber with two smaller fluidic ports within it. One port connects to the loading reservoir, while the other port connects to the chamber. The PCR chamber is also connected to a hydrophobic vent port and to the separation system. The separation system consists of a 5 cm long separation channel connected to the waste, cathode, and anode reservoirs. The PCR chambers and capillary electrophoresis channels are etched into one glass substrate, while the thermal elements (heaters and temperature sensors) are fabricated on a second, flat glass substrate. The RTD elements are fabricated so that they will be inside the PCR chambers after thermal compression bonding of the two substrates to form closed glass chambers and channels.

Microfabrication

Fig. 2 presents a schematic of the process flow used to create the microfluidic PCR-CE chips. To form the channels and chambers (Fig. 2, part I), glass wafers (1.1 mm thick D263, Schott, Yonkers, NY) were cleaned before sputter deposition of a 2000 Å layer of amorphous silicon by DC magnetron sputtering (UHV Sputtering, San Jose, CA). Photoresist (Shipley 1818, Marlborough, MA) was spun on and photolithographically patterned using a contact aligner (Karl Suss, Waterbury Center, VT) and the underlying silicon sacrificial layer was etched

using SF_6 in a parallel-plate reactive ion etching (RIE) system (Plasma Therm, St. Petersburg, FL). Next, the fluidic channels, electrophoresis channels, and PCR chambers were etched to a depth of 36 μm in a mixture of 1:1:2 HF:HCl:H$_2$O. The remaining silicon was removed using an SF_6 etch, and the valve and vent reservoirs in addition to the wells at the cathode, anode, and waste locations were drilled using a rotary drill press with a micrometer stage for alignment. Last, the edges of the etched and drilled wafers were cut using a dicing saw as shown in Fig. 1.

To form the integrated RTD and heating elements (Fig. 2, part II), 1.1 mm D263 glass wafers were coated on one side with 100 Å of Ti and 2000 Å of Pt (UHV Sputtering). Thick photoresist (Shipley SJR 5740, Marlborough, MA) was spun on and patterned using a contact aligner and the metal was etched using hot aqua regia (3:1 HCl:HNO$_3$, 90 °C) to form the RTD elements. This side of the wafer was next blanket coated with 2000 Å of SiO$_2$ using plasma-enhanced chemical vapor deposition (PECVD, PEII-A, Technics West, San Jose CA). The edges of the wafer were shadow-masked with microscope slides to avoid SiO$_2$ deposition on the RTD leads. Next, the back side of the wafer was sputter-coated with 100 Å of Ti and 2000 Å of Pt to form an electroplating seed layer (Perkin-Elmer, Wellesley, MA). Thick photoresist was spun on this side, patterned, and hard baked at 70 °C for 2 h. Gold was electrodeposited onto the Ti–Pt seed layer at 4.3 mA cm^{-2} for 20 min to a 5 μm thickness using a gold sulfite plating solution (Technic TG 25 E, Anaheim, CA). The photoresist was removed and the backside was re-patterned using thick
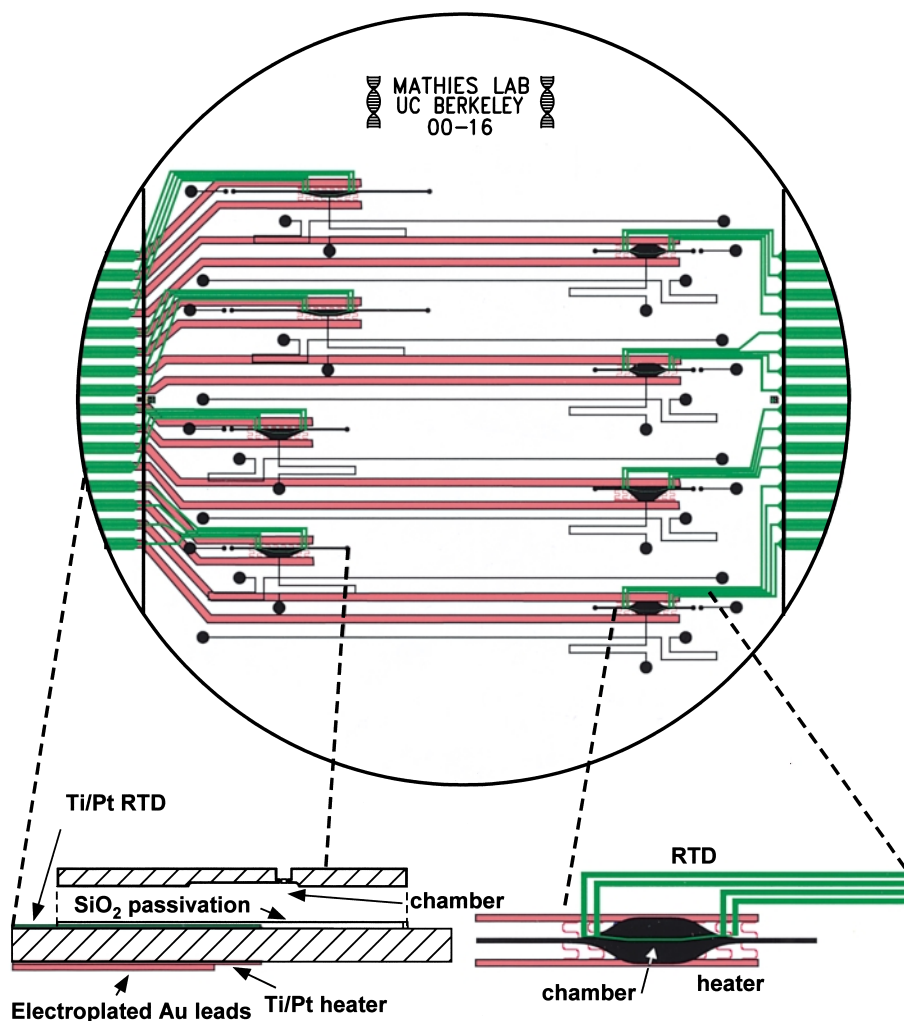

Fig. 1 Overview of the PCR-CE mask design including microfabricated heaters and resistance temperature detectors (RTDs). Bottom left, an expanded view of a partial cross-section of the device, showing the two glass layers and their relative alignment. Bottom right, an expanded top view of the chamber area, showing the chamber, the RTD, and the heater.

photoresist. The heating elements were etched into the Ti–Pt seed layer using an ion beam etching system (Veeco Instruments, Plainview, NY). Last, 3000 Å of SiO$_2$ was deposited over the heaters and leads using PECVD (Technics PEII-A). The edges of this side of the wafer were also shadow-masked to allow ohmic contact to the heater leads. Fig. 3 presents a perspective view of the PCR chamber and temperature control elements, as well as a scanning electron micrograph (SEM) of one of the completed RTDs. The drilled channel wafer was thermally bonded to the RTD/heater wafer using a programmable vacuum furnace (Centurion VPM, J.M. Ney,
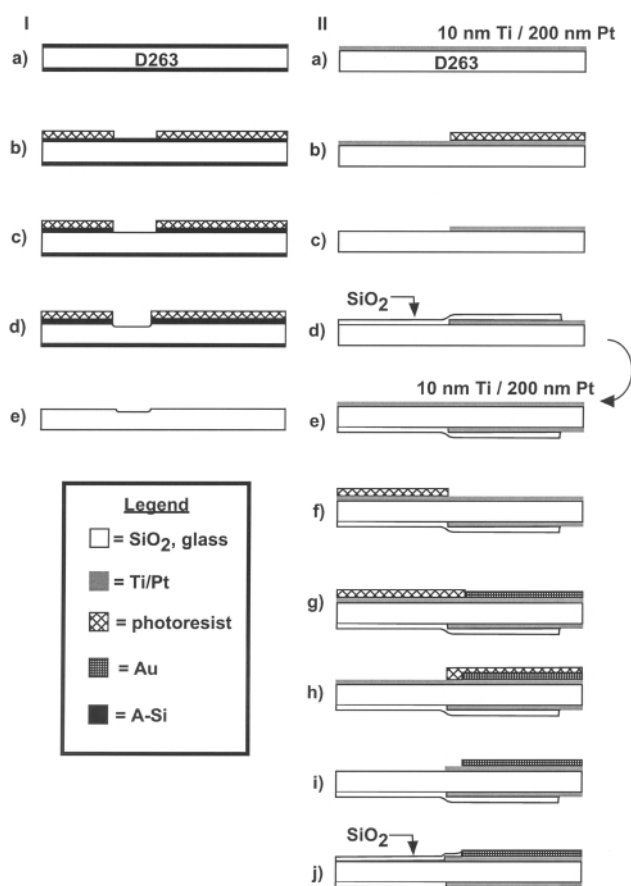
Yucaipa, CA). The channel surfaces were coated using a modified version of the Hjertén coating protocol.[22] Further microfabrication details can be found elsewhere.[23]

The materials used were picked for their properties as well as their compatibility with the glass fabrication process. Titanium and platinum have proven to be among the few metals capable of withstanding thermal compression bonding without significant resistivity changes due to oxidation or other material failures. Gold is among the metals with the lowest bulk resistivities, making it ideal for low-resistance contacts. In addition, gold electroplating processes are very well documented and characterized.

The valves and vents were actuated using a custom-built aluminium manifold which vacuum seals to the chip during use and uses pressure and vacuum controlled from external solenoid valves. Valves and hydrophobic vents were installed after fabrication. 2.5 mm diameter latex membranes (thickness approx. 150 μm) were attached to 2.5 mm id o-rings (Apple Rubber Products, Lancaster, NY) with epoxy, and the structures were placed around the projections on the valve manifold. Hydrophobic vent material consisting of circular sections of a 1.0 μm pore size hydrophobic membrane (Millipore, Bedford, MA) were installed concurrently. Further details of valve and vent construction will be found in our earlier publications.[19,20]

RTD calibration

The RTDs were calibrated after bonding and channel coating by immersing the entire chip into a water bath and ramping the temperature from room temperature to 100 °C. The PC board connector used for all experiments applied 1 mA of current through the outside pairs of leads and sensed voltage on the inside pair of leads for each four-lead RTD. Voltage as a function of temperature from room temperature to 100 °C was recorded and the resistance at each temperature point was then calculated by dividing by the applied current. The data were fit to the Calendar Van-Dusen Equation, which for temperatures above 0 °C assumes a quadratic form:

$$R_T = R_0(1 + AT + BT^2)$$

where T is the temperature, R_T is the resistance at temperature T, and R_0 is the resistance at 0 °C. From the fit data, the A and B constants were determined and used in later experiments. Using the fit constants, R_0 was determined based on the room temperature at the start of each experiment and used for that experiment. This dynamic calculation prevented the need for recalibration before each run.

Instrumentation

The PCR chambers were thermally cycled with a LabVIEW program (National Instruments, Austin, TX). A precision current source (National Instruments SC-2042-RTD) was used to supply 1 mA to the RTD of interest and the voltage across the RTD was collected and filtered using an active lowpass filter (National Instruments 5B backplane). Temperature control was accomplished through a proportion/integrator/differentiator (PID) module within the LabVIEW program. The DAC output used to control the heater passed through a current source circuit to supply the power necessary to drive the heaters.

The CE separation medium was 0.75% (w/v) hydroxyethyl cellulose (HEC) in 1X Tris acetate EDTA (TAE) buffer with 1 μM thiazole orange. The PCR-CE chips were filled with HEC by forcing the solution through the entire microfluidic system using a syringe. The gel was evacuated from the PCR chambers and the sample bus by applying vacuum at the valve reservoir, forming a passive barrier to the flow of reagents from the PCR chamber into the separation channel during amplification. The

Fig. 2 Fabrication scheme for the PCR-CE device. Part I (left) shows the fabrication process flow for the channel layer. Part II (right) shows the fabrication of the heaters and RTDs on the bottom layer.
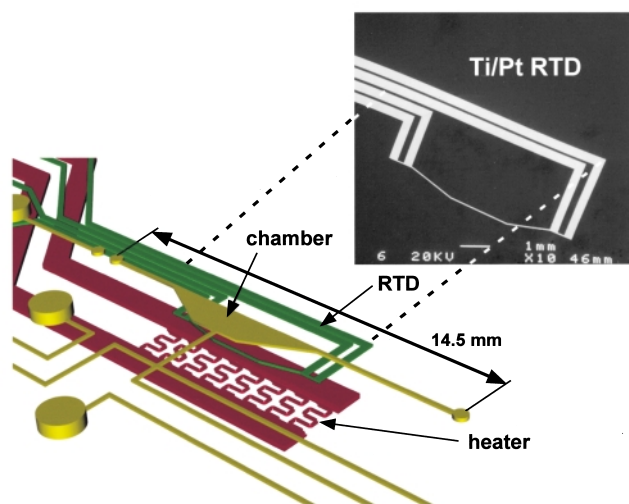

Fig. 3 Perspective view of the integrated microsystem showing relative positions of the PCR chamber, RTD, and heater. Inset: SEM showing detail of the RTD structure.

valve and vent manifolds were sealed to the chip by applying vacuum to each manifold and the sample was introduced at one of the sample reservoirs with a pipette. The valve was opened by applying vacuum to the appropriate port on the valve manifold, and vacuum was simultaneously applied to the corresponding hydrophobic vent. Air pressure applied at the sample reservoir forced the sample through the valve and into the PCR chamber. The valve was then closed (10–15 psi†) to prevent sample movement during heating. Bubble-free loading was consistently achieved using this methodology.

PCR amplification and capillary electrophoresis

The template for multiplex PCR amplification consisted of human genomic DNA control sample (Centre d'Estude du Polymorphisme Humain (CEPH) DNA, Coriell Cell Repositories, Camden , NJ). The two sets of primers for the centromeric alphoid repeat sex determination assay each amplify a unique section of either the X or Y chromosome. The sequences (X3: 5′-TATTTGGACTCTCTCTGAGGA, X4: 5′-TTCTACTA-CAAGGGTGTTGCA, Y3: 5′-GTGTATTCACCTCCGG-GAG, Y4: 5′-ACAAAAGGTTCAATTCTGTGAG), from the work of Neeser and Liechtigallati,[24] amplify a 157 bp and a 200 bp fragment of the X and Y chromosomes, respectively. The PCR mixture (50 μL) consisted of Taq MasterMix kit (1X PCR buffer, 1.5 mM $MgCl_2$, 200 μM each dNTP, and 2.5 units of *Taq* polymerase, Qiagen, Valencia, CA), 1.5 μM BSA, 0.25 μM each primer, and 5 ng of template DNA. The solution was made fresh daily and kept on ice. The thermal cycling protocol applied to the chip consisted of 20 cycles of 95 °C for 5 s, 53 °C for 15 s, and 72 °C for 10 s, for a total cycling time of 10 min. After amplification, the sample was injected into the CE separation channel by applying a field strength of 112 V cm^{-1} and separated by applying a field strength of 236 V cm^{-1} with backbiasing in the sample and waste arms. Excitation of the dye-labeled DNA fragments was achieved with a 488 nm Ar-ion laser at a power of 450 μW focused at the end of the separation channel. The fluorescence was collected through a confocal microscope (Carl Zeiss, Thornwood, New York) into a photomultiplier tube (R943-02, Hamamatsu, Bridgewater, New Jersey), and the digital pulses generated by the PMT were discriminated and stretched using a photon counting unit (PCU3866, Hamamatsu) and directly counted using a National Instruments DAQ board (PCI-MIO-16E-1).

Results and discussion

The design of the heaters and temperature detectors in our new PCR-CE device is intended to create uniform heating and fast thermal response times while minimizing the power required to operate the device. The heater, shown in Fig. 1, is a parallel serpentine design. This design sets the resistance to the desired value (8 Ω) while allowing current to continue to flow should one of the individual heating elements fail. The rounded turns of the heater allow for uniform current density, minimizing the chances for failure due to local heating and electromigration. The heater leads are fabricated using a gold electroplating process. The greater thickness is necessary to lower the current density in the leads (2 × 10^4 A cm^{-2}) so that they do not heat during thermal cycling of the heaters. The average resistance for the gold electroplated leads was 0.3 ± 0.1 Ω, while the average resistance for the heaters was 8.0 ± 0.7 Ω. Since Joule heating depends linearly on resistance, the power dissipation ratio between the heaters and leads was approximately 27. The resistance of both the heaters and the RTDs changed after

† 1 psi ≈ 6894.757 Pa.

thermal compression bonding of the two substrates. The resistance decreased in all cases after thermal treatment, as would be expected for annealing of a thin metal film. Visual inspection of the metal layers after bonding revealed color changes and small areas of hillocking within the film. Previous work provides evidence of oxidation of Ti and diffusion of Ti into Pt layers at temperatures above 450 °C and times longer than 2 h.[25,26] Since our bonding is conducted at temperatures above this and for longer times, observations of such changes in film morphology are consistent with this explanation.

The RTDs are designed to enable fast thermal response and accurate temperature measurement. The location of the RTD inside the PCR chamber allows for direct thermal measurement, at the point of interest, instead of on the backside of the device as in our earlier design. The section of the RTDs within the chambers is small to allow for fast thermal response time. This both increases the accuracy of the measurement and reduces the time lag between the application of the temperature and sensing. In addition, the four-lead RTD is more accurate than the two-lead RTD, since it separates the effects of Joule heating in the device from actual temperature change within the PCR chamber.[27] Fig. 4 presents a typical calibration curve for the RTD-heater device. The resistance response as a function of temperature is very close to linear, as would be expected for a Pt RTD over this narrow temperature range. Due to the small surface area of the RTD elements, the thermal response time is very fast. Typical observed response times, measured as the difference between the time a temperature step was applied and a 1/e change in measured temperature, were on the order of 0.1 s. This is a factor of four longer than the theoretical thermal diffusion time from the heater, but a factor of 50 shorter than the smallest thermal residence time used in our experiments.

Fig. 5 presents the temperature profile as a function of time for 20 cycles of thermal cycling conducted using the RTD/heater chip. It was necessary to spike the temperature at the heater to achieve the correct temperature within the chamber, but since the temperature was controlled from the RTD, this was accomplished automatically. The indicated variation in temperature within each temperature step is 0.5 °C. Although this is larger than for the commercial thermocouple used originally, the accuracy is still high enough to allow successful amplification. Further optimization in the active filtering and the thermal tuning parameters used to control the PCR reaction should decrease the variations. The heating and cooling rates for the thermal cycling both exceed 10 °C s^{-1}; the heating rate approaches 20 °C s^{-1} at an applied power of 1 W. Transition times were 1.1 s from 53 °C to 72 °C, 1.2 s from 72 °C to 95 °C, and 3.0 s from 95 °C to 53 °C. Active cooling, performed by air
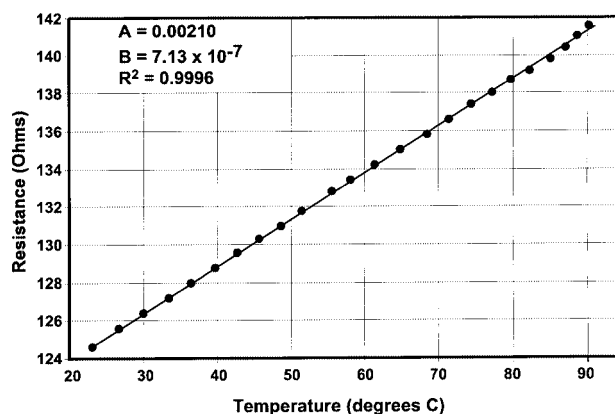
Fig. 4 Calibration curve for the RTD. Temperature as a function of resistance was fit with a high degree of confidence (R^2 = 0.9996) to a quadratic function. The small value of the quadratic constant *B* is consistent with the high degree of linearity as expected for a Pt RTD over such a narrow temperature range.

blown across the chip during the cooling steps was used to increase the cooling rates. The remarkably fast thermal cycling, especially in the heating steps, can be attributed to better thermal contact between the heater and the chip surface than in previous designs. The new heating and cooling rates are the fastest thermal cycling ever achieved on a microfabricated contact PCR-CE device.

Fig. 6 presents results of a successful multiplex PCR amplification of human genomic DNA using this PCR-CE microdevice. The time to perform 20 cycles of PCR amplification was 10 min. After thermal cycling, the PCR products were immediately injected and separated on the electrophoresis channel. The entire analysis was complete in 15 min. Two separate amplifications were performed, the first using control DNA from a female subject, and the second using control DNA from a male subject. In the first case, one peak is seen, indicating the presence of only the X chromosome. In the second case, two peaks are detected, one each for the X and Y chromosomes. Comparison with a DNA sizing ladder run separately allows peak assignments of the expected 157 bp and 200 bp products. The difference in peak areas between the X- and Y-chromosome products is due to the different melting temperatures, and therefore amplification efficiencies, of the two primer sets at the single annealing temperature (53 °C) used in the amplifications. The genomic DNA template is not seen in the electropherograms because its large size inhibits injection onto the separation channel. The template amount used was 5 ng, a moderate amount of DNA. However, the results presented here as well as previous work[19,20] indicate that lower sample

concentrations are possible. The signal-to-noise ratio indicates that reduction of the template concentration by a factor of 5 while performing only 20 cycles of amplification would be possible, bringing the template concentration to levels typically used in forensic investigations. An increase in the number of cycles should also increase the signal, and therefore allow detection of smaller template concentrations.

The integrated PCR-CE microdevice developed here improves over our previous designs, and demonstrates further advantages over both conventional devices and other integrated devices. The volume (200 nL) used here is the smallest volume to date, allowing sample and reagent conservation. The thermal cycling times are the fastest ever demonstrated in a contact PCR-CE device. Although PCR chambers microfabricated in silicon have faster heating and cooling rates, they do not provide the advantage of integrated sensitive CE analysis. Microfabricated stand-alone PCR reactors also require larger volumes, from 500 nL[15] to 28 μL.[28] The current device also allows for multiplex reactions in a single PCR chamber; unlike real-time PCR, the number of possible simultaneous amplification products is determined by primer design and PCR reaction conditions, rather than the spectral overlap of different dyes used to label different products. This allows for much more complicated multiplex assays to be conducted in this device. In addition, our PCR-CE device is capable of generating PCR products from small amounts of human genomic DNA, a critical step toward a forensic identification or medical diagnostics device. Our device is re-useable, requiring only rinsing with water between runs. However, for future clinical diagnostic use it will be desirable to develop fabrication methods and materials that are inexpensive and disposable. Future work will determine the thermal anisotropy of this new design, optimize the PCR chamber design based on this analysis, and determine the optimal number of cycles. Addition of further sample prepara-
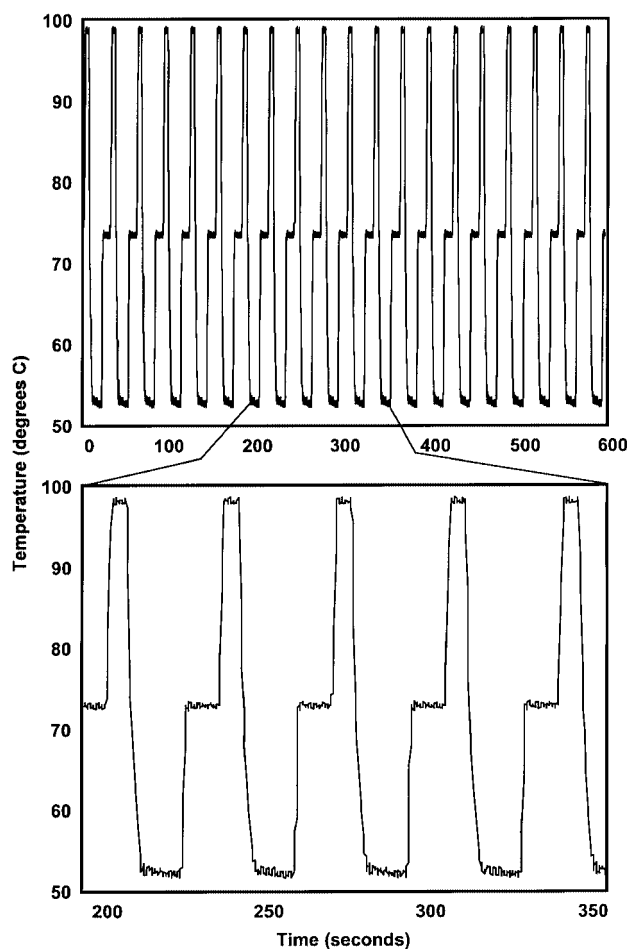

Fig. 5 Thermal cycling of the integrated PCR-CE device. Top, all 20 cycles of thermal cycling used in these experiments. 20 cycles are complete in 10 min. Bottom, an expanded view of 5 individual cycles, showing the very fast heating and cooling (~20 °C s⁻¹) obtained with the microfabricated heaters. Transition times were 1.1 s from 53 to 72 °C, 1.2 s from 72 to 95 °C, and 3.3 s from 95 to 53 °C.
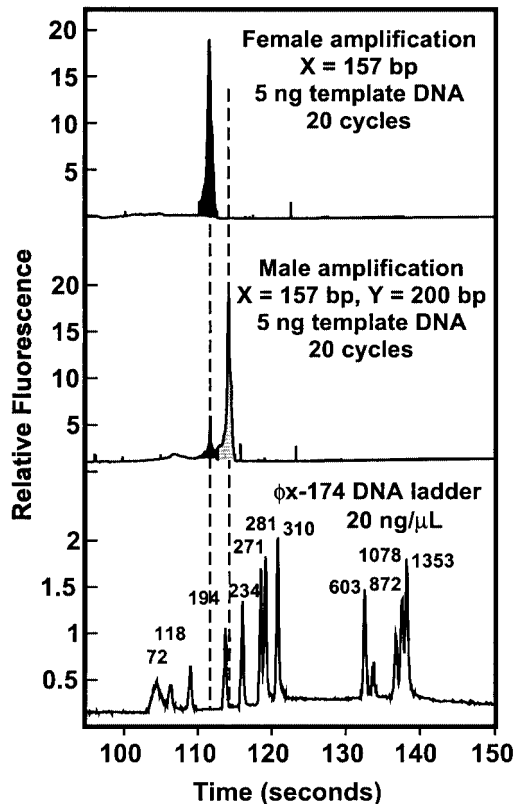

Fig. 6 Multiplex sex determination from human genomic DNA using the PCR-CE microdevice. Top: amplification from female DNA. Only the 157 bp peak representing amplification from the X chromosome is seen. Middle: amplification from male DNA; both the 157 bp X-chromosome and the 200 bp Y chromosome amplicons are observed. Bottom: DNA sizing ladder for amplicon size reference, run separately on the same device.

tion steps, such as genomic DNA isolation, is also possible, yielding a device for use in clinical, forensic, or other environments.

Conclusions

A fully integrated microfluidic system to load, PCR amplify, and analyze nanoliter volumes of DNA has been constructed with integrated microfabricated heating and temperature sensing elements. These elements significantly improve the thermal cycling efficiency and heating and cooling rates over previous levels. This system demonstrates high-speed PCR amplification and detection in a time of only 15 min. Successful multiplex amplification of sex markers from human genomic DNA is achieved. This device points the way to an integrated genomic analysis microsystem for use in forensic and point-of-care medical diagnostic environments.

Acknowledgements

References

1   *Micro Total Analysis Systems*, ed. J. M. Ramsey and A. van den Berg, Kluwer, Dordrecht, The Netherlands, 2001.
2   K. Mullis, F. Faloona, S. Scharf, R. Saiki, G. Horn and H. Erlich, *Cold Spring Harbor Symp. Quant. Biol.*, 1986, **51**, 263.
3   M. A. Northrup, M. T. Ching, R. M. White and R. T. Watson, *DNA Amplification with a Microfabricated Reaction Chamber. Proceedings 7th International Conference on Solid-State Sensors and Actuators*, Yokahama, Japan, 1993, pp. 924–926.
4   P. Wilding, M. A. Shoffner and L. J. Kricka, *Clin. Chem.*, 1994, **40**, 1815.
5   A. T. Woolley, D. Hadley, P. Landre, A. J. deMello, R. A. Mathies and M. A. Northrup, *Anal. Chem.*, 1996, **68**, 4081.
6   P. Belgrader, J. K. Smith, V. W. Weedn and M. A. Northrup, *J. Forensic Sci.*, 1998, **43**, 315.
7   J. H. Daniel, S. Iqbal, R. B. Millington, D. F. Moore, C. R. Lowe, D. L. Leslie, M. A. Lee and M. J. Pearce, *Sens. Actuators, A*, 1998, **71**, 81.
8   P. Wilding, L. J. Kricka, J. Cheng, G. Hvichia, M. A. Shoffner and P. Fortina, *Anal. Biochem.*, 1998, **257**, 95.
9   L. C. Waters, S. C. Jacobson, N. Kroutchinina, J. Khandurina, R. S. Foote and J. M. Ramsey, *Anal. Chem.*, 1998, **70**, 5172.
10 L. C. Waters, S. C. Jacobson, N. Kroutchinina, J. Khandurina, R. S. Foote and J. M. Ramsey, *Anal. Chem.*, 1998, **70**, 158.
11 N. Y. Zhang and E. S. Yeung, *J. Chromatogr., B: Biomed. Appl.*, 1998, **714**, 3.
12 N. Y. Zhang, H. D. Tan and E. S. Yeung, *Anal. Chem.*, 1999, **71**, 1138.
13 S. Poser, T. Schulz, U. Dillner, V. Baier, J. M. Kohler, D. Schimkat, G. Mayer and A. Siebert, *Sens. Actuators, A*, 1997, **62**, 672.
14 M. A. Northrup, B. Benett, D. Hadley, P. Landre, S. Lehew, J. Richards and P. Stratton, *Anal. Chem.*, 1998, **70**, 918.
15 R. P. Oda, M. A. Strausbauch, A. F. R. Huhmer, N. Borson, S. R. Jurrens, J. Craighead, P. J. Wettstein, B. Eckloff, B. Kline and J. P. Landers, *Anal. Chem.*, 1998, **70**, 4361.
16 M. S. Ibrahim, R. S. Lofts, P. B. Jahrling, E. A. Henchal, V. W. Weedn, M. A. Northrup and P. Belgrader, *Anal. Chem.*, 1998, **70**, 2013.
17 M. U. Kopp, A. J. de Mello and A. Manz, *Science*, 1998, **280**, 1046.
18 I. Schneegaß, R. Bräutigam and J. M. Köhler, *Lab Chip*, 2001, **1**, 42.
19 E. T. Lagally, P. C. Simpson and R. A. Mathies, *Sens. Actuators, B*, 2000, **63**, 138.
20 E. T. Lagally, I. Medintz and R. A. Mathies, *Anal. Chem.*, 2001, **73**, 565.
21 R. C. Anderson, X. Su, G. J. Bogdan and J. Fenton, *Nucleic Acids Res.*, 2000, **28**, e60.
22 S. Hjerten, *J. Chromatogr.*, 1985, **347**, 191.
23 P. C. Simpson, A. T. Woolley and R. A. Mathies, *Biomed. Microdevices*, 1998, **1**, 7.
24 D. Neeser and S. Liechtigallati, *J. Forensic Sci.*, 1995, **40**, 239.
25 W. Qu, W. Wlodarski and M. Austin, *Microelectron. J.*, 2000, **31**, 561.
26 H. Esch, G. Huyberechts, R. Mertens, G. Maes, J. Manca, W. De Ceuninck and L. De Schepper, *Sens. Actuators, B*, 2000, **65**, 190.
27 J. H. Moore, C. C. Davis and M. A. Coplan, *Building Scientific Apparatus: A Practical Guide to Design and Construction*, Reading, MA, 1989.
28 T. B. Taylor, E. S. Winn-Deen, E. Picozza, T. M. Woudenberg and M. Albin, *Nucleic Acids Res.*, 1997, **25**, 3164.